npj | flexible electronics

Article

Published in partnership with Nanjing Tech University

https://doi.org/10.1038/s41528-024-00302-6

Inherently integrated microfiber-based flexible proprioceptive sensor for feedback-controlled soft actuators

Hwajoong Kim[1], Hyunbin Na[1], Seungbeom Noh[1], Shinwon Chang[2], Jinho Kim[1], Taejune Kong[1], Gyowook Shin[2], Chankyu Lee[3], Seonggyu Lee[1], Yong-Lae Park[2], Sehoon Oh[1] & Jaehong Lee[1]

For the accurate and continuous control of soft actuators in dynamic environments, the movements of the soft actuators must be monitored in real-time. To this end, various soft actuators capable of self-monitoring have been developed by separately integrating sensing devices into actuators. However, integrating such heterogeneous sensing components into soft actuators results in structural complexity, high manufacturing costs, and poor interfacial stability. Here, we report on intelligent pneumatic fiber-reinforced soft actuators with an inherent flexible proprioceptive sensor that uses only the essential components of typical fiber-reinforced soft actuators. The inherent flexible proprioceptive sensor is achieved by leveraging two parallel conductive microfibers around an elastomeric chamber of the soft actuator, which simultaneously acts as both a capacitive bending sensor and radial expansion limiting fibers of typical fiber-reinforced soft actuators. The proprioceptive soft actuator exhibits excellent mechanical actuation up to 240° bending motion and proprioceptive sensing performance with high sensitivity of 1.2 pF rad^{-1}. Mathematical analysis and simulations of the soft actuator can effectively predict the bending actuation and capacitive responses against input pressures. We demonstrate that proprioceptive soft actuators can be used to construct a soft gripping system and prosthetic hand which express various hand gestures and perform dexterous manipulation with real-time proprioceptive sensing capability.

Soft robots are emerging as alternatives to rigid robots in various robotic applications owing to their outstanding adaptability[1,2] to diverse shapes and surface morphologies. For the development of soft robots, various types of soft actuators composed of compliant materials, such as pneumatic[3–6], hydraulic[7,8], electrical[9,10], magnetic[11,12], thermal[13,14], and ionic soft actuators[15,16], have been intensively developed. In particular, pneumatic soft actuators have been widely used for soft robots owing to their benefits, including large-scale deformations[17], simple designs[18–20], lightweights[21], and inherent safety[22,23]. These advantages of soft actuators can be considered fundamental requirements for their application in real-world scenarios.

Another important requirement for intelligent soft actuating systems is a sensory feedback control of the actuators for reliable operation in dynamic environments. Based on feedback control, soft actuators can accurately maintain their actuating performance, independent of unexpected external disturbances from the surroundings. To this end, embedded sensing of soft actuators which ensures real-time monitoring of their actuation is fundamentally essential[24,25]. However, realizing pneumatic soft actuators with embedded sensing has been challenging. In this context, there have been a few studies that additionally embedded or attached heterogeneous sensing components, such as resistive[26–28], capacitive[29–32], magnetic[33], inductive[34], and optical strain sensors[35–37], to pneumatic soft actuators for monitoring of their physical deformation during the actuation. Chen et al. [38] demonstrated a bidirectional bending soft actuator integrated with optical waveguide sensors. A pneumatic soft actuator with a feedback control system was also developed using commercial bending sensors by Gerboni et al.[39]. Despite extensive efforts to develop diverse types of self-sensing soft actuators based on embedded or attached heterogeneous sensing components, these methods can induce several limitations in practical applications. Embedding additional heterogeneous sensing elements into pneumatic soft actuators undeniably raises the structural complexity of the entire system. This is not

[1]Department of Robotics and Mechatronics Engineering, Daegu Gyeongbuk Institute of Science and Technology (DGIST), 333 Techno jungang-daero, Hyeonpung-eup, Dalseong-gun, Daegu, Republic of Korea. [2]Department of Mechanical Engineering, Seoul National University, 1 Gwanak-ro, Gwanak-gu, Seoul, Republic of Korea. [3]University of California, Berkeley, CA, USA. e-mail: jaelee@dgist.ac.kr

only due to the intricate wiring layout required for these sensing components, but also because of the multitude of rigid soldering points needed between the sensing components and their corresponding wires[40,41]. Such structural complexity and the rigid soldering points can considerably restrict the broader applicability and usability of the soft actuator system in real-world applications. The increased structural complexity also leads to complicated manufacturing processes potentially, resulting in the elevation of both material and production costs[42]. Moreover, a structural and mechanical mismatch between the soft body of the actuator and the integrated heterogeneous sensors into the soft actuator can frequently induce poor interfacial stability at the interface during the operation of the actuating system, subsequently reducing the stability and durability of the proprioceptive soft actuators[43]. Therefore, the simultaneous realization of a pneumatic soft actuator and a proprioceptive sensing capability without any heterogeneous sensing components in a soft actuator is highly beneficial for intelligent soft actuating systems with closed-loop feedback control. Nevertheless, such intelligent pneumatic soft actuators that provide inherent proprioceptive sensing without heterogeneous sensing components have not yet been developed.

In this work, we report on a strategically rational design for intelligent fiber-reinforced pneumatic soft actuators with an inherently integrated microfiber-based flexible proprioceptive sensor. Through our innovative design approach, we developed a proprioceptive soft actuator that successfully accomplishes real-time proprioception even without any heterogeneous sensing components within the system. To develop the inherent microfiber-based proprioceptive sensor, two parallel conductive microfibers are strategically incorporated as part of the radial expansion limiting fibers in a fiber-reinforced soft actuator, allowing them to also act as a microfiber-based capacitive bending sensor. Thanks to the conductive microfibers which perform the two roles in the actuator, the developed soft actuator exhibits not only excellent fiber-reinforced actuation performance but also a proprioceptive sensing capability against bending actuation using only the essential components of a typical fiber-reinforced soft actuator. Based on the innovative design approach, our soft actuators could effectively overcome the practical limitations of previous soft actuators by simplifying the system layout and complicated fabrication processes, and alleviating the poor interfacial stability between soft actuators and integrated heterogeneous sensing components. An analytical expression and finite element simulation model are developed to verify the correlations between the mechanical actuating performance of the soft actuators and capacitive sensing behaviors of the inherent flexible proprioceptive sensors. The proprioceptive soft actuator provides negligible hysteresis and high durability regarding both mechanical actuation and capacitive sensing capability, demonstrating its high stability. We also achieve a closed-loop feedback control system of the soft actuator based on the proprioceptive sensing capability, which can compensate for unintended external loadings and maintain the desired actuation in a dynamic environment. We demonstrate the proprioceptive soft actuator to construct a versatile soft gripping system and soft prosthetic hand with proprioceptive sensing capability.

Results

Design and working mechanism of intelligent proprioceptive soft actuator

A schematic illustration of the structure for the intelligent proprioceptive soft actuator is presented in Fig. 1a. The proprioceptive soft actuator consists only of the essential components required for a typical fiber-reinforced pneumatic soft actuator without any additional heterogeneous elements; an elastomeric chamber, axial strain-limiting fiber, and radial expansion limiting fibers. The radial expansion limiting fibers were helically wound in a crossing fashion around the elastomeric chamber, which effectively restricts the radial expansion of the actuator under an applied input pressure. The axial

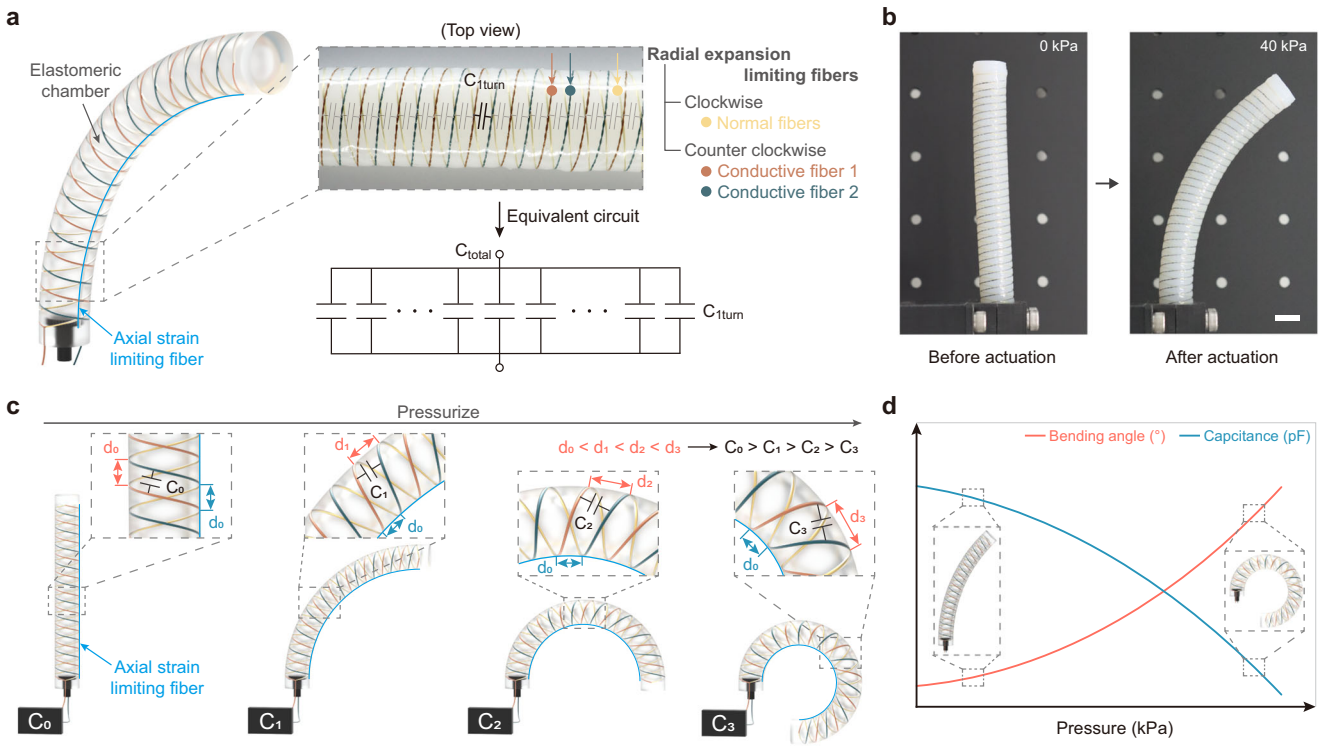

Fig. 1 | Design and working mechanism of the intelligent proprioceptive soft actuator. a Schematic illustration of a fiber-reinforced pneumatic soft actuator with proprioceptive sensing capability. The magnified photograph and circuit show the top-view of the proprioceptive soft actuator and the equivalent circuit of the proprioceptive bending sensor in the soft actuator, respectively. **b** Photograph showing the fabricated proprioceptive soft actuator in the unpressurized (0 kPa) and pressurized (40 kPa) states. Scale bar, 10 mm. **c** Schematic illustration describing the proprioceptive sensing mechanism of the soft actuator upon applied pneumatic pressure. **d** Conceptual graph showing the bending actuation of the soft actuator and corresponding capacitive response of the proprioceptive bending sensor with increasing applied pressure.

strain-limiting fiber was placed along the chamber in the longitudinal direction, which partially restrict the longitudinal deformation of the actuator under an applied pressure. The detailed fabrication process for the proprioceptive soft actuator is shown in Supplementary Figs. 1 and 2. The fabricated soft actuator could be efficiently operated with a bending actuation under an applied pneumatic pressure, thanks to the radial expansion limiting fibers and axial strain-limiting fiber (Fig. 1b). When a pneumatic pressure is applied to the inside of the fiber-reinforced soft actuator, the elastomeric chamber of the actuator is inflated only in the longitudinal direction due to the constraint of its radial expansion by the radial expansion limiting fibers. Simultaneously, the axial strain-limiting fiber partially inhibits the longitudinal growth of the soft actuator along the limiting fiber, promoting its bending actuation[44]. To confirm the uniformity of the bending actuation along the longitudinal direction of the soft actuator, we evaluated the distances between the conductive microfibers within the actuator under various bending angles, as shown in Supplementary Fig. 3. To endow the actuator with a proprioceptive sensing capability, we also designed an inherently integrated microfiber-based capacitive bending sensor without any additional components in the fiber-reinforced soft actuator. As described in Fig. 1a, the microfiber-based capacitive bending sensor was incorporated by employing two parallel conductive microfibers with a radius of 100 μm as a part of the radial expansion limiting fibers, instead of normal nylon fibers. In particular, the two parallel conductive microfibers were used as radial expansion limiting fibers helically wound in clockwise (or counterclockwise). Our design for the proprioceptive fiber-reinforced soft actuator was thoughtfully established through comparative analysis with another potential design (Supplementary Fig. 4). Because the two parallel conductive microfibers are separated from each other, a microfiber-based capacitive bending sensor can be formed by the two conductive microfibers acting as the two electrodes of a capacitor. Figure 1c shows a schematic illustration describing the bending sensing mechanism of the inherent proprioceptive sensor in the soft actuator. As the bending actuation of the soft actuator continues with increasing input pneumatic pressure, the distance between the two conductive radial expansion limiting fibers wound in parallel around the elastomeric chamber asymmetrically increases. The asymmetrical change in the winding structure of the two conductive microfibers under bending actuation is attributed to the non-uniform elongation of the soft actuator in the longitudinal direction resulting from the axial strain-limiting fiber. As described in Fig. 1c, the distance between the two conductive microfibers on the concave surface (d_0) is efficiently maintained during the bending actuation of the actuator due to the restriction of the axial strain-limiting fiber. However, the distance between the two conductive microfibers on the convex surface increases according to the longitudinal elongation of the soft actuator under the bending actuation (d_0 to d_3). The asymmetrical increase in the distance between the two conductive microfibers under bending actuation decreases the capacitance of the capacitive bending sensor in the proprioceptive soft actuator. The equivalent circuit of the proprioceptive bending sensor can be described as a parallel connection of several unit capacitive sensors corresponding to a single turn of two conductive microfibers in the soft actuator (Fig. 1a). By measuring the capacitance change between the two conductive microfibers, the bending deformation of the soft actuator can be monitored in real-time during its actuation. Therefore, the intelligent fiber-reinforced soft actuator provides proprioceptive sensing capability without any heterogeneous component for the actuator (Fig. 1d and Supplementary Video 1). The presented design approach significantly enhances system simplicity by eliminating the need for additional sensing components and the corresponding complex wiring layout typically required in such systems. Notably, given that the conductive radial expansion limiting fibers can be directly extended to act as interconnects for the microfiber-based sensors, our proprioceptive soft actuator eliminates the need for any rigid soldering within the system. This feature significantly enhances the practical stability of soft actuators in real-world applications (Supplementary Table 1).

Mechanical behavior of the proprioceptive pneumatic soft actuator

The bending angle of the proprioceptive soft actuator under a bending actuation is defined as the included angle between the two normal lines at the proximal and distal tips of the actuator as shown in Fig. 2a. Figure 2b shows the change in the bending angle of a soft actuator, fabricated with a diameter of 14 mm and helical pitch of 3 mm, upon the applied internal pressure. As the input pressure applied to the soft actuator increased, the soft actuator was bent due to the partial stretching restriction of the axial strain-limiting fiber, resulting in an increase in the bending angle of the soft actuator. A numerical simulation based on the finite element method (FEM) provided excellent agreement with the experimental results over the entire pressure range, verifying the mechanical behavior of the fiber-based soft actuator under the applied pressure (Fig. 2b, c). A detailed explanation of the numerical simulation is given in the Supplementary Information (Supplementary Figs. 5-7 and Supplementary Video 2). In addition, the actuating behavior of the intelligent fiber-based soft actuator was analytically verified through mathematical analysis. As described in the free body diagrams of the soft actuator in Fig. 2d, at a constant internal pressure, the soft actuator reaches a static-state bending deformation, which results from the effect of the fiber reinforcement and the equilibrium between two bending moments within the system: moment M_p generated by the internal pressure, and moment M_t generated by the restoring force of the elastomeric chamber[45]. Considering the equilibrium between the two bending moments at an arbitrary point in the cross-section including the inner surface of the distal tip (Fig. 2e), the relationship between the applied internal pressure P_{in} and the bending angle of the soft actuator θ can be derived as follows:

$$P_{in} = 4A_1\theta - 6A_2\theta^2 + 10A_3\theta^3 - \cdots \tag{1}$$

$$A_i = \frac{\frac{\mu}{L_0^i}\int_0^{2\pi}\int_0^t \left\{\left(r_{in}+t\right) + \left(r_{in}+\tau\right)\sin\phi\right\}^{i+1}\left(r_{in}+\tau\right)d\tau d\phi}{\pi r_{in}^2(r_{in}+t)} \tag{2}$$

where, A_i indicates a variable coefficient for each term in Eq. (1), determined by the geometrical dimensions and material properties of the soft actuator, μ denotes the shear modulus of the elastic material, L_0 is the initial length of the soft actuator, r_{in} and t are the inner radius and thickness of the soft actuator, respectively, ϕ indicates the direction of an arbitrary infinitesimal area where the internal pressure is applied (Fig. 2e), and τ means the minimum distance from the inner surface of the side wall of the soft actuator to an arbitrary infinitesimal area where the elastic stress is applied to the side wall (Fig. 2e). The detailed calculations for the relationship between the applied internal pressure and the bending angle of the actuator are described in the Supplementary Information. The calculated bending angle of the soft actuator against the applied internal pressure showed a good agreement with the experimental results for the entire actuating range (Fig. 2b). The orthogonal coordinate for the bending trajectory of the distal tip of the soft actuator under an applied internal pressure (Fig. 2f) can also be calculated using a geometric approach as follows:

$$\left(x, y\right) = \left(R\sin\theta, R(1-\cos\theta) = \left(\frac{L_0\sin\theta}{\theta}, \frac{L_0(1-\cos\theta)}{\theta}\right)\right. \tag{3}$$

where, R is the radius of curvature of the soft actuator under bending actuation. The calculated and simulated bending trajectory of the soft actuator under the applied internal pressure closely matched the experimental results, demonstrating the validity of the analytical and simulated expectations (Fig. 2g). To characterize the output force of the soft actuator, the isometric and isotonic responses of the actuator were

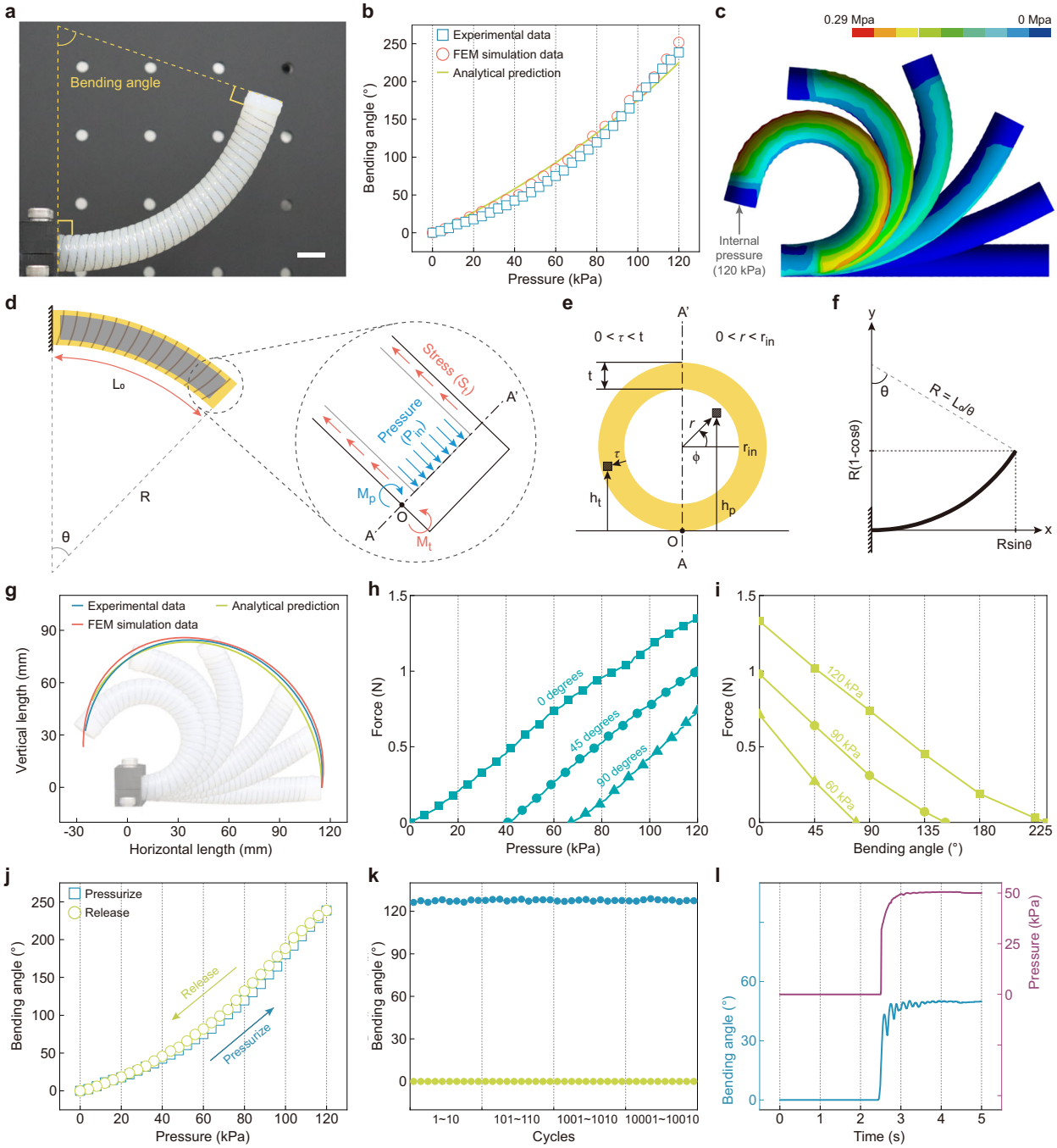

Fig. 2 | Mechanical characterization of the proprioceptive pneumatic soft actuator. a Photograph showing the definition of the bending angle of the soft actuator under bending actuation. Scale bar, 10 mm. **b** Bending angle response of the soft actuator according to applied internal pressure (blue squares). The red circles and solid line show the expected response of the soft actuator based on an FEM simulation and analytical model. **c** Superimposed FEM images of the soft actuator at different bending angles. The principal stress range of the elastomeric chamber is indicated in the legend. Schematic illustration showing **d** free body diagram of the soft actuator under bending actuation, **e** cross-section of the soft actuator including the inner surface of its distal tip, and **f** bent soft actuator described in orthogonal coordinates. **g** Distal tip trajectory of soft actuator with bending angle from 0 to 250°. Photographs of the soft actuator at the different bending angles are overlaid in the graph. **h** Isometric and **i** isotonic responses of the soft actuator measured at the distal tip of the actuator. **j** Relative change in the bending angle of the soft actuator during the consecutive pressurizing-releasing cycle. **k** Durability test of the soft actuator upon repeated applied pressure of 90 kPa over 10,000 cycles. **l** Response time of the soft actuator against 50 kPa of the applied pressure.

evaluated by measuring the force generated at the distal tip of the actuator during the bending actuation (Fig. 2h, i and Supplementary Fig. 9). The isometric response of the soft actuator was tested by measuring the output force generated at the distal tip under a constant bending angle (0, 45, and 90°) while input pressure increased from 0 to 120 kPa. The isometric response showed parallel lines for several bending angles, demonstrating the stable bending actuation of the actuator (Fig. 2h). In a similar manner, the isotonic response of the soft actuator was evaluated by measuring the output force at the distal tip according to different bending angles under a constant input pressure (60, 90, and 120 kPa) as shown in Fig. 2i. Despite the nonlinear behavior of the elastomeric chamber of the soft actuator, the isotonic response provided the

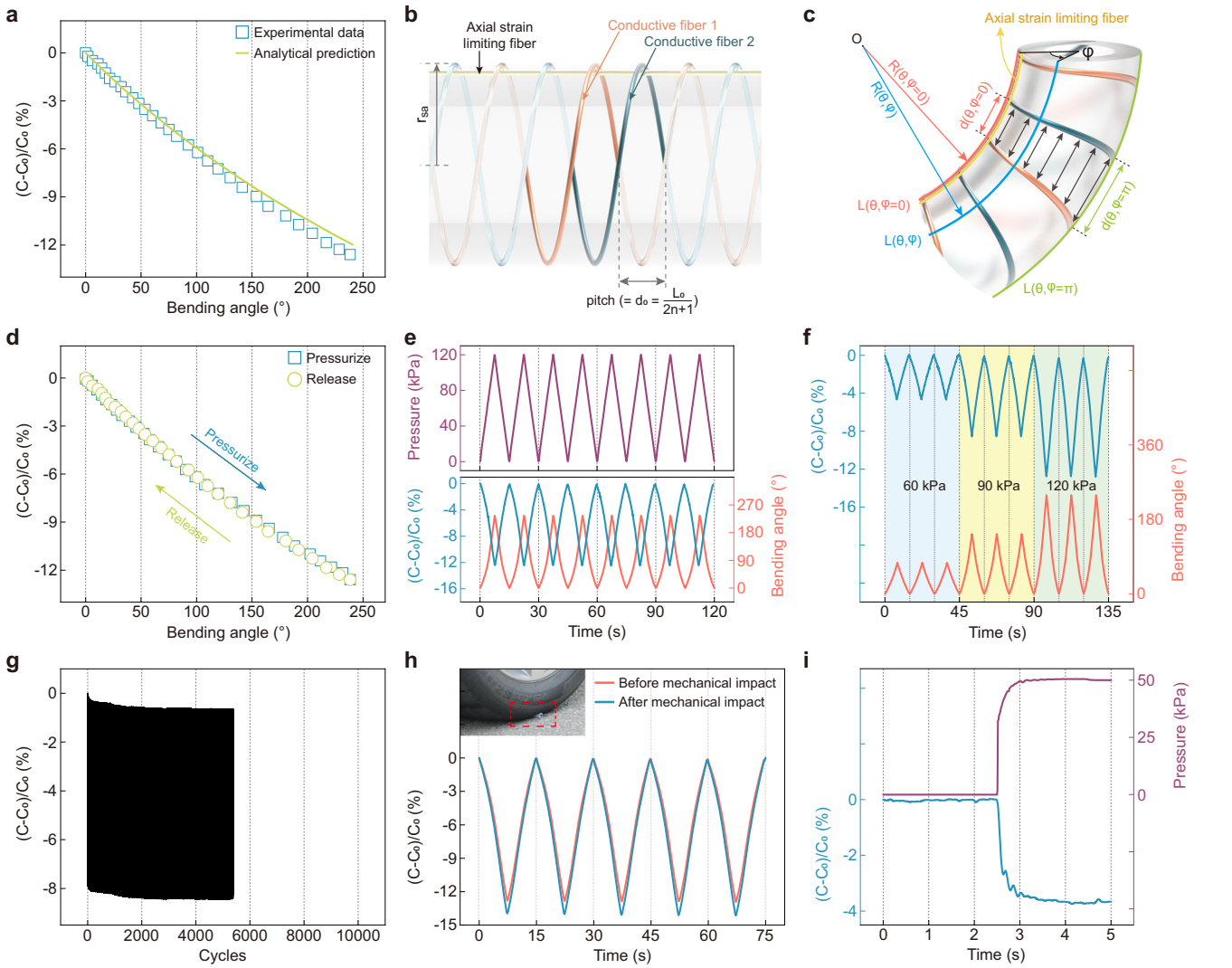

Fig. 3 | Proprioceptive sensing performance of soft actuator. a Capacitive response of the proprioceptive bending sensor according to bending angle of soft actuator. The solid line shows the analytical prediction of the sensor response based on a mathematical model. **b** Schematic illustrations of the two conductive microfibers helically wound around the elastomeric chamber of the soft actuator in unpressurized state. **c** Schematic illustration showing the structural change of the two conductive microfibers of the proprioceptive sensor in a pressurized state. **d** Relative change in the capacitance of the proprioceptive bending sensor during a pressurizing-releasing cycle. **e**, **f** Bending angle changes of the soft actuator and corresponding normalized capacitance changes of the proprioceptive sensor upon repeated pressures of 60, 90, and 120 kPa. **g** Capacitive response of the proprioceptive bending sensor upon repeated internal pressure of 90 kPa over 10,000 cycles. **h** Relative change in the capacitance of the sensor under repeated pressure of 120 kPa before and after large mechanical impact by a car. **i** Capacitive response of the proprioceptive sensor against step function of internal pressure applied to the soft actuator.

maximum achievable output force of the soft actuator for a particular input pressure under zero bending[46].

The mechanical stability and durability of the proprioceptive soft actuator were also investigated. Figure 2j shows a slight hysteresis of the bending actuation of the soft actuator upon consecutive pressurizing-releasing cycle. Hysteresis is one of the well-known limitations of soft pneumatic actuators, which is generally explained to be caused by mechanical mismatches and friction between several different components of the soft actuator[43]. However, the presented proprioceptive soft actuator does not contain any additional heterogeneous components other than the essential parts, minimizing the friction and heterogeneity between the several components in the soft actuator. Thanks to this, our soft actuator barely led to hysteresis during the consecutive bending actuation, demonstrating the high mechanical stability of the actuator. Moreover, the negligible hysteresis of the soft actuator was also verified even under diverse conditions such as various maximum internal pressures, flow rates, and pressurizing-releasing cyclic tests (Supplementary Fig. 10 and Supplementary Videos 3 and 4). Owing to its high stability, the soft actuator also effectively maintained the bending actuation without any considerable degradation even after an intensive 10,000 cyclic test with 90 kPa of applied internal pressure, demonstrating the high mechanical durability of the soft actuator as shown in Fig. 2k. In addition, despite the time-dependent behavior of the viscoelastic elastomer, the soft actuator exhibited fast response time (71 ms) and recovery time (38 ms) against 50 kPa of applied internal pressure, as shown in Fig. 2l and Supplementary Fig. 11, respectively[47,48]. Both the response and recovery times were defined as the duration until the bending actuation of the soft actuator reaches 63.2% of the steady-state deformation under the applied internal pressure.

Microfiber-based flexible proprioceptive sensing capability of intelligent proprioceptive soft actuator

As described in Fig. 1c, the soft actuator can perceive its bending deformation based on the capacitive response of the inherent microfiber-based proprioceptive sensor composed of two parallel conductive microfibers

wound around the actuator. Figure 3a and Supplementary Fig. 12 show the relative change in the capacitance of the proprioceptive bending sensor, fabricated with a diameter of 14 mm and helical pitch of 3 mm, according to the bending actuation of the soft actuator. The capacitance of the bending sensor in the soft actuator gradually decreased under the bending deformation. The negative response of the capacitive bending sensor is attributed to the increase of distance between the two parallel conductive microfibers of the sensor under the bending deformation of the actuator. The two parallel conductive microfibers of the sensor are helically wound around the elastomeric chamber, initially maintaining a constant distance between the two microfibers throughout the entire soft actuator (Fig. 1c and Fig. 3b). When the soft actuator is bent upon the applied internal pressure, locally gradual tensile stretching in the actuator occurs except for the longitudinal part along the axial strain-limiting fiber, which leads to an asymmetric increase in the distance between the two conductive microfibers (Fig. 3c). Therefore, the capacitance of the proprioceptive bending sensor decreases upon the bending deformation of the soft actuator. The working mechanism of the proprioceptive bending sensor can be mathematically described by considering the structural behavior of the helically wound two conductive microfibers under bending actuation. The capacitance C of the proprioceptive bending sensor according to the bending angle of the bent soft actuator can be calculated as follows:

$$C(\theta) = (2n-1)02\pi \int \frac{\pi\varepsilon(r_{sa}-r)}{\ln\left(\frac{\theta}{r(2n+1)}\sqrt{\left(\frac{L_0}{\theta}\right)^2 + 2\left(r_{sa}-r\right)\left(\frac{L_0}{\theta}+r_{sa}-r\right)(1-\cos\varphi)}\right)} d\varphi \quad (4)$$

where n indicates the total number of turns for the two parallel conductive microfibers wound around the elastomeric chamber, ε denotes the permittivity between the two conductive microfibers, and r_{sa} and r are the outer radius of the soft actuator and radius of the conductive microfiber, respectively. θ and φ mean the bending angle and azimuthal angle of the soft actuator, and L_0 is the initial length of the helically wound capacitive sensor. Detailed calculations of the capacitive response of the sensor are described in the Supplementary Information. The expected capacitive response of the proprioceptive bending sensor calculated using the analytical model exhibited a good agreement with the experimental results, as shown in Fig. 3a.

Figure 3d and Supplementary Fig. 15 show the capacitive response of the proprioceptive bending sensor upon a consecutive pressurized-unpressurized cycle of the soft actuator. For the entire internal pressure range, the proprioceptive bending sensor in the soft actuator exhibited a negligible hysteresis of the capacitive response, demonstrating the high stability of the sensor (Supplementary Fig. 16a). Because the working mechanism of the proprioceptive bending sensor directly relies on the mechanical behavior of the soft actuator, the high stability of the sensor (due to the lack of hysteresis) is mainly attributed to the small mechanical hysteresis of the soft actuator. The bending sensor successfully maintained its capacitive response and negligible hysteresis even under higher pressure flow rates, as described in Supplementary Fig. 16b. Thanks to the high stability, the soft actuator provided a clear and stable response for both its bending actuation and proprioceptive sensing during repeated pressurizing-releasing cycles with different applied pressures of 60, 90, and 120 kPa (Fig. 3e, f). In addition, the stable capacitive response and negligible hysteresis of the proprioceptive bending sensor in the soft actuator were successfully maintained without any considerable degradation even after an intensive cyclic test (10,000 cycles with an internal pressure of 90 kPa), as shown in Fig. 3g and Supplementary Figs. 16c and 17. Because the proprioceptive soft actuator is fully composed of elastomeric materials and flexible microfibers, the soft actuator remained intact and stably maintained its actuating and proprioceptive sensing capabilities even after a great mechanical impact by a car, showing the high durability of the soft actuator (Fig. 3h and Supplementary Fig. 18). The proprioceptive bending sensor of the soft actuator also exhibited a rapid response and recovery time of 71 and 82 ms against a step pressure applied into the soft actuator, which is comparable with previous pneumatic actuators (Fig. 3i and Supplementary Fig. 19)[49].

Characterization of the microfiber-based flexible proprioceptive sensor

To further investigate the effects of the structural parameters of the soft actuator on its main performance, soft actuators with different diameters of the elastomeric chamber and a constant pitch (distance between the helically wound two conductive microfibers) of 3 mm were prepared, as shown in Supplementary Fig. 20a. Figure 4a and Supplementary Video 5 show that the actuating capability of the soft actuator slightly increases with its larger diameter. This increase in actuating capability is attributed to the increased area of the inner surface of the soft actuator with a larger diameter. The increased inner surface area of the side wall in the soft actuator leads to a higher total pneumatic force applied to the inner surface under a certain level of internal pressure. Because the side wall of the fiber-reinforced soft actuator is physically restricted by the radial expansion limiting fibers, the pneumatic force applied to the inner surface of the restricted wall mainly contributes to reinforcing the longitudinal elongation of the actuator[45]. Therefore, a higher pneumatic force applied to the inner surface of the side wall in a soft actuator with a larger diameter leads to a greater elongation of the soft actuator in the longitudinal direction, resulting in a larger bending actuation. Due to the higher pneumatic force in the soft actuator at a specific internal pressure, the soft actuator with the larger diameter generated a higher output force at its tip under a fixed bending angle (Fig. 4b and Supplementary Fig. 21a). In addition, the larger diameter of the soft actuator, the higher sensitivity of the proprioceptive sensor against the bending actuation of the actuator (Fig. 4c and Supplementary Fig. 21b), because the larger diameter of the soft actuator leads to a larger tensile strain on the convex surface of the actuator upon its bending actuation (Supplementary Fig. 21c). The larger tensile strain on the convex surface also induces a larger increase in the distance between the two conductive microfibers on the convex surface, resulting in a greater decrease in the capacitance of the proprioceptive sensor under the bending actuation. Regardless of its diameter, the soft actuator exhibited small hysteresis and high durability (Supplementary Fig. 21d–f). In a similar manner, soft actuators with different pitches of helically wound conductive microfibers (2, 3, and 4 mm) and a constant diameter of 14 mm were also evaluated, showing the negligible effect of the pitch on the main performance of the soft actuator (Supplementary Figs. 22 and 23 and Supplementary Video 6). In addition to bending actuation, stretching and helical actuation can also be achieved by leveraging the axial strain-limiting fiber in the soft actuator. When the axial strain-limiting fiber is not included in the soft actuator, the actuator is stretched only in the longitudinal direction with respect to the increasing internal pressure (Fig. 4d, Supplementary Fig. 24, and Supplementary Video 7). The stretching actuation of the actuator results from the absence of longitudinal restriction of the actuator that the axial strain-limiting fiber could induce. Furthermore, the soft actuator successfully achieved helical actuation by locating the axial strain-limiting fiber in the helical layout around the actuator (Fig. 4e, Supplementary Fig. 25, and Supplementary Video 7). By strategically adjusting the arrangement of the fibers in the soft actuator, we also designed a multimotion proprioceptive soft actuator capable of integrating three distinct types of actuations including extension, twisting-extension, and bending, into a single device (Fig. 4f). In particular, the extension actuation was achieved by removing the axial strain-limiting fiber, as demonstrated in Fig. 4d, in the region 1 of the soft actuator. In addition, the twisting-extension actuation was accomplished in region 2 of the actuator by using only the radial expansion limiting fibers in one direction, excluding both the counter radial expansion limiting fibers and the axial strain-limiting fiber. The bending actuation in region 3 was realized in the same manner with the soft actuator presented in Fig. 1a. Based on the integration of the three distinct actuations, the fabricated multimotion soft actuator successfully achieved complex deformation, as shown in Fig. 4g and Supplementary Video 8. To measure the local and global complex deformations of the multimotion soft actuator, we

established a local field proprioceptive sensing system by strategically arranging conductive microfiber electrode pairs. To this end, three pairs of microfiber electrodes were integrated in a single actuator as the radial expansion limiting fibers in one direction, which simultaneously act as individual proprioceptive sensors for the distinct actuation regions in the multimotion soft actuator (Supplementary Fig. 26 and Fig. 4f). In particular, the capacitive response of the proprioceptive sensor 3 correlated with the bending actuation in the region 3 of the actuator. In a similar manner, the proprioceptive sensor 2 and 1 could detect the twisting-extension actuation in region 2 and extension actuation in region 1, respectively (Fig. 4h).

Because the output capacitance of the proprioceptive bending sensor can be unintentionally affected by conductive objects in the vicinity of the

Fig. 4 | Characterization of proprioceptive soft actuator. a Bending actuation of the proprioceptive soft actuators with different diameters of 10, 14, and 18 mm and a constant pitch of 3 mm in response to increasing internal pressure. **b** Forces generated at the distal tips of soft actuators with the different diameters under fixed bending angle of 0° and increasing internal pressure. **c** Capacitive responses of the proprioceptive bending sensors in the soft actuators with the different diameters according to bending angle of the bent actuators. **d** Schematic illustration of the soft actuator without the axial strain-limiting fiber (left) and the capacitive response of the proprioceptive sensor in the soft actuator against stretching actuation under applied internal pressure (right). The inset shows the stretching actuation of the soft actuator without the axial strain-limiting fiber. **e** Schematic illustration of the soft actuator where the axial strain-limiting fiber is helically wound around the actuator (left) and proprioceptive sensing response of the soft actuator with increasing internal pressure (right). The inset shows the helical actuation of the soft actuator with the helically wound axial strain-limiting fiber. **f** Schematic illustrations showing the design of the multimotion soft actuator. Dashed box includes the layout of fiber reinforcements for each actuation region. **g** Photographic images illustrating the complex deformation of the multimotion soft actuator that combines extension, extension-twisting, and bending actuation. **h** Capacitance changes of the three local proprioceptive sensors in the multimotion soft actuator during repeatedly applied pressures of 120 kPa. **i**–**k** Normalized capacitance changes of the proprioceptive bending sensor of the soft actuator during repeated bending actuation in the vicinity of the various objects.

soft actuator, the capacitive response of the sensor was investigated with various objects including paper, polypropylene, glass, steel, aluminum plate, and a hand, as shown in Supplementary Fig. 27a. The proprioceptive sensor maintained its output capacitance near non-conductive objects such as paper, polypropylene, and glass plate (Supplementary Fig. 27b, d, e) However, the overall output capacitance of the sensor during same bending actuation was negatively shifted in the vicinity of conductive objects such as steel, aluminum plate, and a human hand (Supplementary Fig. 27b, d, f). This shift in the capacitance of the sensor was attributed to the interfered electric field between the two conductive microfibers by the conductive objects. Despite the shift in the output signal, the relative change in the capacitance of the proprioceptive sensor was successfully reproducible regardless of the type of object near the sensor, demonstrating the high stability of the sensor against the surrounding environment (Fig. 4i–k and Supplementary Fig. 27c).

Model-based two-degree-of-freedom control to compensate for the internal pressure against unintended external loading

To exploit the potential of the newly developed soft actuator, we designed a fast and robust Two-Degree-Of-Freedom (TDOF) motion controller. The TDOF controller comprises a Disturbance Observer (DOB), Proportional-Integral-Derivative (PID) control, and Feedforward control, as depicted in Fig. 5a, where $G_{n,\,soft}$ represents the nominal model of the soft actuator, G_{soft} is the actual soft actuator, and Q is a low pass filter[50,51]. The DOB in this control scheme compensates for the external loads based on the model. A detailed explanation of the control algorithm and system identification process is given in the Supplementary Information. To design the TDOF controller for the proprioceptive soft actuator, we first estimated its transfer function through a system identification process performed at a sampling frequency of 12.5 Hz. The frequency response function was obtained from 0.01 to 5 Hz, as illustrated in Fig. 5b. Figure 5c shows that the estimated model matches well with the electrical behavior of a real soft actuator according to a sinusoidal input, although there is a slight difference between the two responses. The control ability of the actuator system to compensate for the internal pressure against unintended external loading was demonstrated by applying external loadings to the soft actuator under bending actuation. The controlled input pressure and capacitance responses of the proprioceptive soft actuator with the TDOF controller under various unintended external loadings are shown in Fig. 5d, e and Supplementary Video 9. The proprioceptive soft actuator with the TDOF maintained a certain internal pressure (36 kPa) and corresponding capacitance with a bending angle of ~43.5° without any external loading from 0 to 20 s. The bending actuation of the soft actuator was successfully maintained even under increasingly applied external loads up to 120 g without considerable deflection (Fig. 5e). Based on the capacitive response of the proprioceptive bending sensor and TDOF controller, the soft actuator could maintain its desired bending actuation by complementing the internal pressure required to compensate for the unintended external loads (Fig. 5d). In contrast, the bending actuation of the soft actuator without the TDOF controller collapsed without any controlled compensation when unintended external loads above 60 g were applied to the actuator (Fig. 5f, g and Supplementary Video 9). Our results demonstrate that the model-based TDOF control designed for the proprioceptive soft actuator can robustly maintain the desired bending actuation against external loadings in a dynamic environment.

Soft robotic demonstrations of proprioceptive soft actuators

To verify the potential of the proprioceptive soft actuator for a human-robot interface, we constructed a soft gripping system and soft prosthetic hand using our soft actuators. Figure 6a shows a soft gripping system fabricated with a robotic arm and three soft actuators with the capability of stable pick-and-place task. When an internal pressure was applied to the three proprioceptive soft actuators in the system, the three actuators were bent evenly, allowing stable gripping of the target objects (Fig. 6b). The proprioceptive bending sensors of the three soft actuators in the gripping system could monitor the bending actuation of the actuators in real-time during the pick-and-place task through the corresponding capacitive response of the sensor (Fig. 6c). We demonstrated that the soft gripping system could successfully convey various objects with different shapes, sizes, and materials such as plastic triangular prisms, cylindrical objects, wood toys, plastic balls, sponges, fitting elements, and paper cups (Fig. 6d and Supplementary Video 10). Moreover, we demonstrated the soft gripping system equipped with closed-loop control, leveraging the proprioceptive sensing of the soft actuator to adjust internal pressure in response to unintended external loading. As shown in Fig. 6e and Supplementary Video 11, the closed-loop control based on the proprioceptive sensing of the soft actuator successfully compensated for external loads applied to the soft actuator in the soft gripping system, maintaining its actuation even under gradually increasing external loads up to 155 g. In comparison, the soft gripping system lacking closed-loop control could only sustain actuation with an external payload of up to 35 g, indicating that the gripping system with the closed-loop control offers 3.3 times higher resistance to external loading (Fig. 6f and Supplementary Video 11).

Furthermore, we implemented the soft prosthetic hand using five proprioceptive soft actuators as fingers of the prosthetic hand, capable of expressing and recognizing a variety of hand gestures based on the proprioceptive sensing capability of the actuator (Supplementary Fig. 28). Figure 7a and Supplementary Video 12 show the soft prosthetic hand expressing the rock-paper-scissors through the selective actuation of the five soft actuators in the prosthetic hand. During the rock-paper-scissors actuation, the soft prosthetic hand continuously and selectively recognized each gesture of the hand by measuring the different capacitive output signals of the five proprioceptive sensors in the soft actuators under the hand gestures (Fig. 7b). In addition, these different capacitive responses of the proprioceptive sensors under the different gestures of the prosthetic hand allowed us to recognize various hand gestures expressed by the prosthetic hand such as sign language (Supplementary Fig. 29 and Supplementary Video 13). In a similar manner, we also demonstrated the capability of the soft prosthetic hand to grip various objects with different geometries, sizes, and weights as shown in Fig. 7c and Supplementary Fig. 30. Because the gripping motion of the soft prosthetic hand relies mainly on the size, shape, and weight of the target object, each finger in the prosthetic hand would have

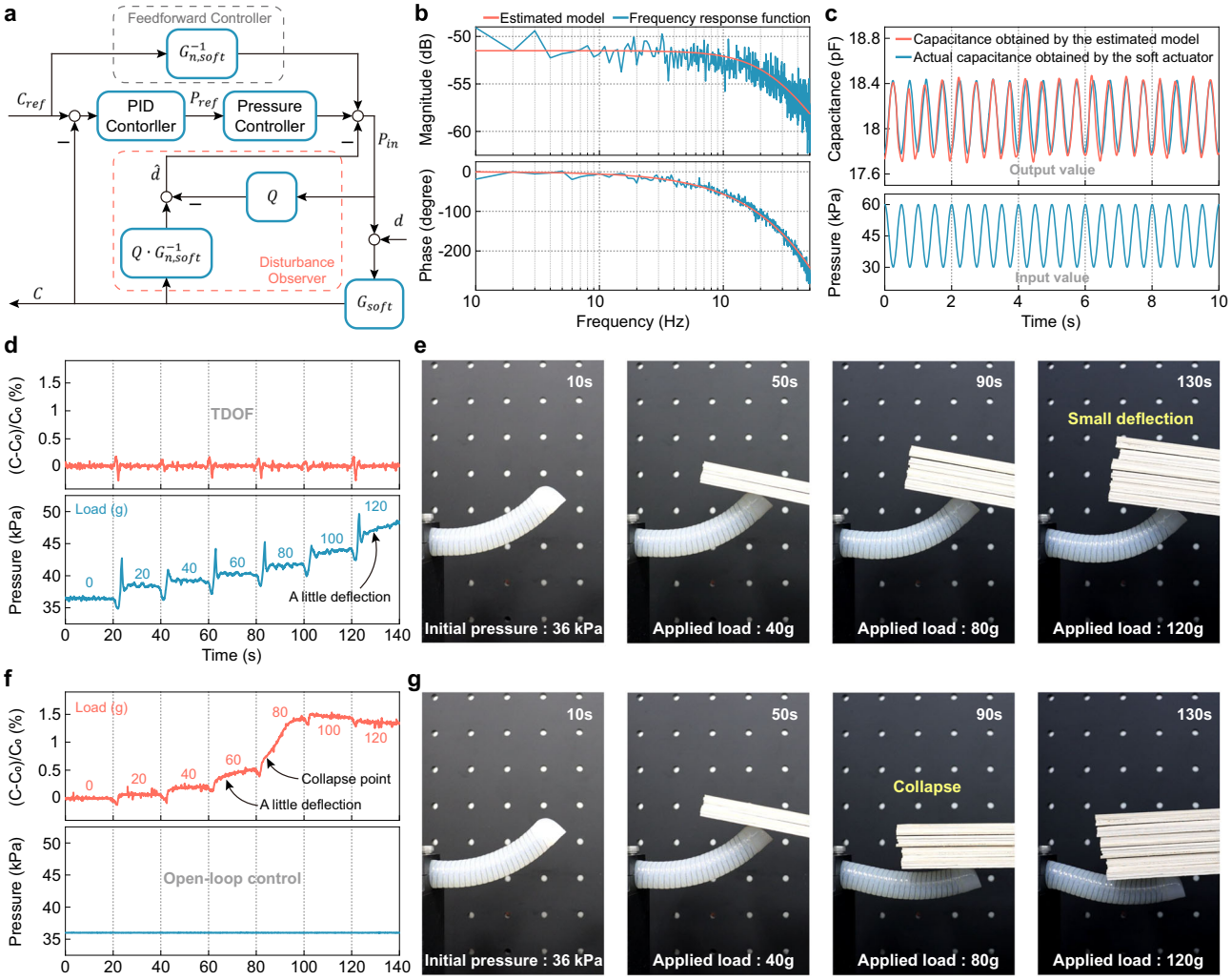

Fig. 5 | Model-based Two-Degree-Of-Freedom (TDOF) control system to compensate for the internal pressure against unintended external loading. a Scheme of model-based TDOF control system. **b** System identification of the soft actuator to achieve the estimated model parameters. **c** Comparison of output responses between estimated model and actual soft actuator. Internal input pressure and capacitance responses of the proprioceptive soft actuator under unintended external loadings with **d** model-based TDOF control system and **f** open-loop control system. **e**, **g** show photographs corresponding to each graph.

different bending actuation according to various target objects. The different bending angles of all the fingers in the soft prosthetic hand gripping several objects could be successfully monitored by measuring the clearly distinguishable capacitive responses of the proprioceptive bending sensors in the five soft actuators (Fig. 7d). By leveraging the distinct capacitive responses of the proprioceptive sensors, various objects gripped by the soft prosthetic hand, such as a balloon, marker pen, apple, and ping-pong ball, could be readily identified as illustrated in Fig. 7e and Supplementary Video 14. Despite employing a straightforward classification approach, the prosthetic hand demonstrated a high accuracy rate of approximately 91% in identifying these four objects across 100 gripping-classification tests (Fig. 7f). We anticipate that the accuracy in classifying gripped objects could be significantly improved by optimizing the algorithms through the application of machine learning techniques.

Discussion

In summary, we present an innovative design for developing a microfiber-based flexible proprioceptive sensor inherently integrated in a soft actuator without the need for any heterogeneous components within the system. The inherent microfiber-based proprioceptive sensor was fabricated by utilizing two parallel conductive microfibers, which simultaneously serve as radial expansion limiting fibers and capacitive proprioceptive sensor in the fiber-reinforced soft actuator. The fabricated proprioceptive soft actuator exhibited excellent mechanical actuation performance and an inherent bending sensing capability. We created an analytical model and numerical simulation that provide precise prediction the mechanical and capacitive sensing behavior of the proprioceptive soft actuator using only measurable parameters without any fitting parameters. The programmable multi-motion soft actuator and proprioceptive local sensing capability were successfully implemented by strategically utilizing the various patterns of fiber reinforcements. Based on the inherent microfiber-based proprioceptive sensor, the soft actuator could be successfully controlled to maintain the desired bending actuation even under an unintended external loading through closed-loop feedback control. We demonstrated that the proprioceptive soft actuator could be used to develop a proprioceptive soft gripping system and soft prosthetic hand capable of gripping and feeling diverse objects.

Compared to previously reported soft actuators with self-sensing capability, our proprioceptive soft actuator offers an advantage in terms of the integrity of the sensing and actuating system. In our design, a flexible proprioceptive sensor is inherently included in a soft actuator with only essential components of typical

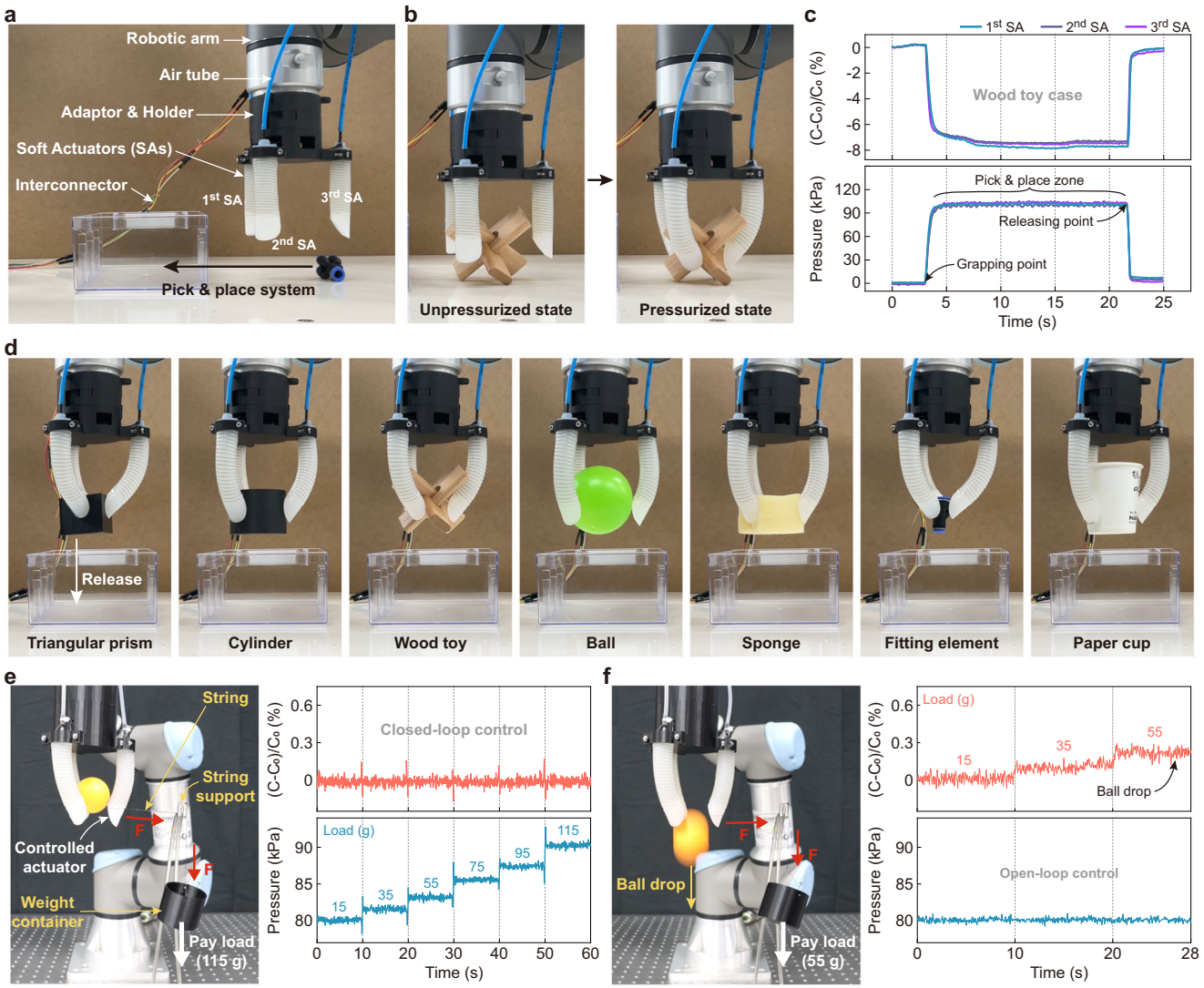

Fig. 6 | Soft gripping system with robotic arm using the proprioceptive soft actuators. a Soft gripping system based on a robotic arm and three proprioceptive soft actuators. **b** Photographs showing the unpressurized and pressurized state of the soft gripping system with a wood toy as a target object. **c** Internal pressure changes of the soft actuators and capacitive responses of the proprioceptive sensors while a wood toy is picked and placed to a specific position with a distance of 12 cm. **d** Pick-and-place tasks of the soft gripping system for various objects including a triangular prism, cylindrical object, wood toy, ball, sponge, fitting element, and paper cup. **e**, **f** Internal input pressure and capacitance responses of the soft actuator in the soft gripping system under unintended external loadings with **e** closed-loop control system and **f** open-loop control system.

fiber-reinforced soft actuators, which eliminates the structural complexity of the existing self-sensing pneumatic soft actuators, including heterogeneous sensing devices. In particular, the presented design strategy not only simplifies the entire system by eliminating intricate internal components, wiring layouts and rigid soldering points, but it also minimizes the poor interfacial stability between the soft body and embedded heterogeneous sensing elements, common challenges in previous self-sensing soft actuators (Supplementary Table 1 and 2). Furthermore, our strategy of exclusively utilizing commercially available materials for the proprioceptive soft actuators has substantial advantages. This approach can significantly decrease both manufacturing and material costs (~0.92 USD per one proprioceptive soft actuator, including the sensing components), effectively lowering the barriers for the commercialization of the presented proprioceptive soft actuator system (Supplementary Table 3). In this context, our proprioceptive soft actuator fabricated through the innovative and rational design strategy achieves significant advancements in terms of system layout complexity, the interfacial stability, and total costs for the actuator system. Moreover, the inherent proprioceptive sensing capability could enhance the overall reliability and stability of soft robotic systems, making them more suitable for real-world applications and human-robot interactions. Future work is, however, required for further improvements. First, the output force generated by the soft actuator can be further increased by adjusting the constituent elastomeric material. The body of a soft actuator can be replaced with other elastomeric materials with a high Young's modulus to achieve a higher output force. Second, a more detailed investigation into various parameters that affects actuating and proprioceptive sensing performance of the presented soft actuator, including the diameter of the fiber reinforcements, the wall thickness and Young's modulus of the elastomeric chamber, can further advance the presented proprioceptive soft actuator. Furthermore, based on these various material and structural parameters, the analytical model for the mechanical and capacitive behavior of the soft actuator can be further refined. Lastly, enhancing the adhesive properties between the microfibers and the elastomeric matrix in the soft actuator can effectively prevent potential drift of the microfibers, which improve the stability of the proprioceptive sensor. We believe

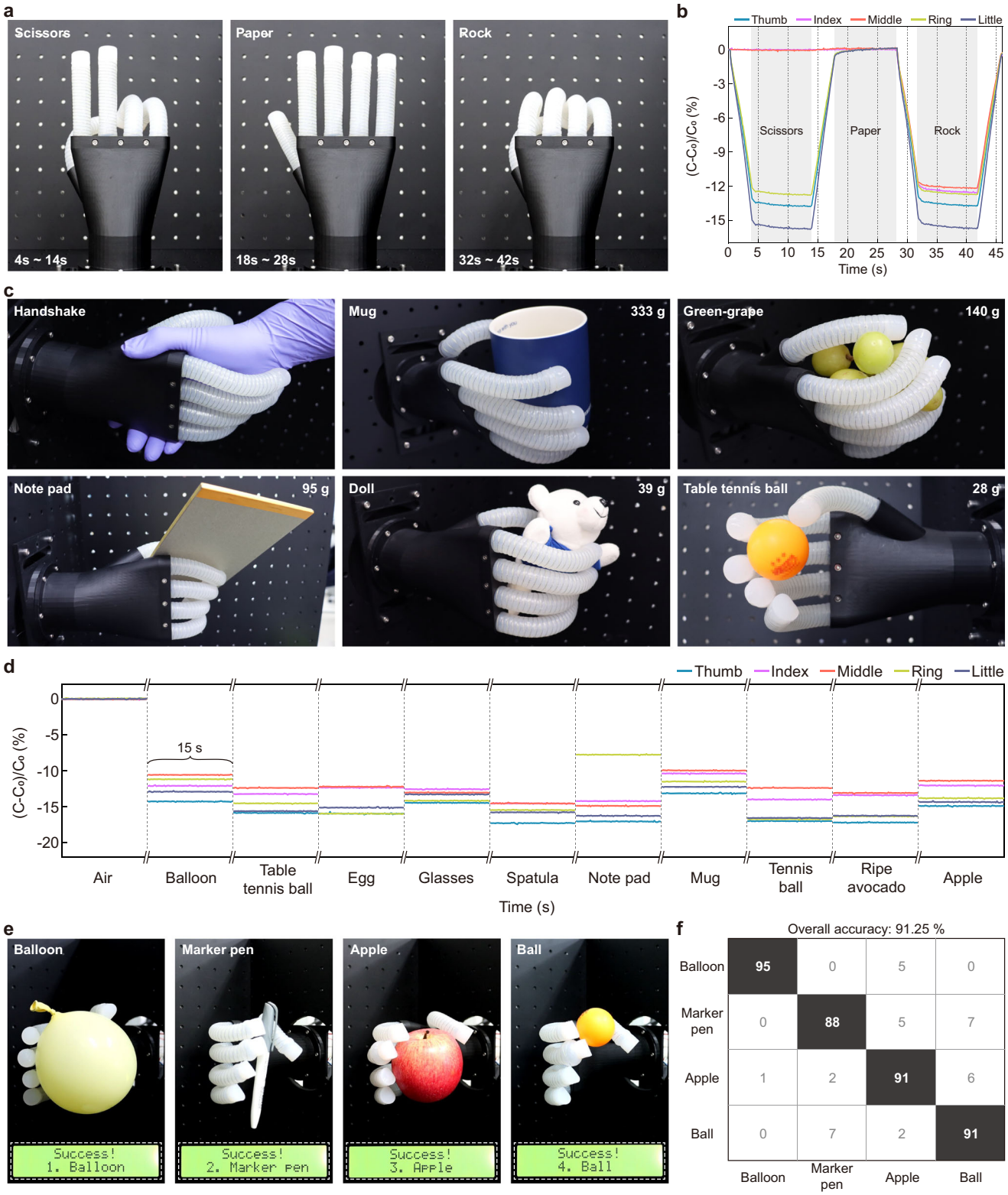

Fig. 7 | Soft prosthetic hand using the proprioceptive soft actuators. **a** Photographs of the soft prosthetic hand expressing the rock-paper-scissors actuation according to finger bending. **b** Different capacitive responses of the five proprioceptive bending sensors with respect to various gestures of rock, paper, and scissors. **c** Photographs showing the capability of the soft prosthetic hand to grip diverse objects such as human hand, mug, green-grape, note pad, doll, and table tennis ball. **d** Clearly distinguishable capacitive responses of the five proprioceptive bending sensors in finger actuators according to the diverse objects grasped by the soft prosthetic hand. **e** Photographs showing the object recognition and classification of the soft prosthetic hand. **f** Classification confusion matrix based on the real-time experimental data.

that our rational and innovative design approach for the proprioceptive soft actuator highlights significance and importance of our work for practical applications of soft actuators.

Methods

Fabrication process of the fiber-reinforced soft actuator with inherent proprioceptive sensor

The fabrication process of the fiber-reinforced soft actuator is divided into four main steps: molding step to make the elastomeric chamber, incorporating step of the axial strain-limiting fiber along the elastomeric chamber in the longitudinal direction, winding step of the radial expansion limiting fibers around the elastomeric chamber in a helical configuration, and encapsulation step of the soft actuator with an elastomeric polymer. For the molding step of the elastomeric chamber, plastic molds for cylindrical objects with helical rips were created using a 3D printer (Ultimaker Ltd., Ultimaker S3) with a tough PLA as shown in Supplementary Fig. 1a. The elastomeric chamber was fabricated by casting a liquid silicone elastomer (Smooth-on Inc., Dragon Skin 10 medium) in a 3D-printed mold with a sacrificial steel rod. After the liquid elastomer in the 3D-printed molds was cured, the steel rod and molds were removed to obtain the elastomeric chamber for the soft actuator with a hollow core (Supplementary Fig. 1b). The open lower end of the elastomeric chamber was capped by placing it in a second 3D-printed mold set containing an uncured elastomeric polymer (Supplementary Fig. 1c). The open upper end of the elastomeric chamber was also capped with plastic tubing to apply the pneumatic input pressure to the soft actuator (Supplementary Fig. 1d). For the bending deformation of the soft actuator, an axial strain-limiting fiber (Sueco Ltd., Kevlar fibers (Para-aramid)) was placed along the pre-defined groove on the elastomeric chamber in the longitudinal direction (Supplementary Fig. 1g). For the fiber reinforcement of the soft actuator, the four radial expansion limiting fibers were wound around the elastomeric chamber along the double helical ribs which acted as a guide groove (Supplementary Fig. 1h to 1l). In particular, two parallel normal microfibers (Sueco Ltd., Kevlar fibers (Para-aramid)) were helically wound clockwise around the elastomeric chamber (Supplementary Fig. 1h, i). In a similar manner, two parallel conductive microfibers (Adafruit Inc., stainless steel microfibers (ADA-640)) were helically wound around the chamber in a counterclockwise direction (Supplementary Fig. 1j–l). Finally, as illustrated in Supplementary Fig. 2, the axial strain-limiting fiber and radial expansion limiting fibers wound around the chamber were secured by encapsulating the entire soft actuator with a thin silicone elastomer layer (Dragon Skin 10 medium).

Mechanical and electrical characterization of the soft actuator and microfiber-based flexible proprioceptive sensor

To apply the internal pneumatic pressure to the soft actuator, a pressure controller (Elveflow Inc., OB1) and commercial compressor (G&P air Inc., EWS30) were used with urethane-based tubes. The input channel of the pressure controller was connected to the compressor and the output channel of the pressure controller was connected to the plastic tubing component of the soft actuator. The pressure controller converted the uncontrolled pneumatic pressure provided by the compressor to controlled pneumatic pressure in order to operate the soft actuator. All of the pressure values in this study indicate the gauge pressure. The bending angle of the bent soft actuator under the applied input pressure was measured by analyzing the images or video frames captured by a DSLR camera (Canon Inc., EOS 90D). To measure the capacitive response of the proprioceptive sensor under the bending actuation of the soft actuator, the two conductive microfibers for the sensor were connected to an inductor-capacitor-resistor (LCR) meter (Keysight-Technologies Inc., E4980AL), measuring the capacitance of the sensor at 300 Hz. Isometric and isotonic force measurements were carried out by measuring the force at the distal tip of the soft actuator using a force meter (Imada Inc., DSV-20N) while increasing the input pressure under a constant bending angle or increasing the bending angle under a constant input pressure.

Soft robotic demonstrations of proprioceptive soft actuators

A robot arm (Universal Robots Inc., UR5e), three pressure regulators (SMC Corp., ITV2030-312CL), and a capacitance detector (Texas Instruments Inc., FEC1004) were used to demonstrate the soft gripping system. The adaptor and holder were designed, and 3D-printed for connecting the robot arm and soft actuators as shown in Fig. 6a. The adaptor was cylindrical with three holders, arranged in a 120° rotation, and three actuators were fastened to the holders with bolts. The capacitance detector in the holder was soldered onto the two conductive microfibers of the proprioceptive bending sensor of the soft actuators to measure the capacitive response of the sensors. To achieve a more stable gripping capability of the system, the proprioceptive soft actuators in the system were fabricated with different structural parameters (an actuator length of 84 mm, pitch of 2.5 mm, and elliptical cross-section with a height of 19 mm and a width of 24 mm). In addition, the shape of the distal tip of the soft actuator was changed from an elliptical cylinder to an elliptical wedge to increase the contact area between the soft actuators and target objects, inducing a high frictional force during the gripping task. The internal pressures of the three soft actuators could be modulated by three regulators in parallel, and each regulator was connected to the pressure sources. The pressure regulators and robotic arm were independently controlled using Arduino Uno R3, and proprietary software provided by Universal Robots Inc., respectively. To implement the pneumatic soft prosthetic hand, five proprioceptive soft actuators were integrated with a 3D-printed rigid palm. The proprioceptive soft actuators in the soft prosthetic hand were fabricated with a constant diameter of 18 mm and pitch of 3 mm. The lengths of the soft actuators in the prosthetic hand were 110 mm for the middle finger, 100 mm for the index and ring fingers, and 85 mm for the thumb and little finger. The two conductive microfibers comprising the proprioceptive bending sensor in the soft actuator were connected to an LCR meter (Keysight-Technologies Inc., E4980AL) to measure the capacitance of the bending sensor. Each soft actuator which acts as a finger for the soft prosthetic hand was controlled by a pressure controller (Elveflow Inc., OB1) to grip several target objects.

Data availability

All data generated or analyzed during this study are included in this published article and supplementary information files.

Code availability

All codes that support the findings of this study are available from the corresponding authors upon reasonable request.

Received: 2 September 2023; Accepted: 24 February 2024;
Published online: 07 March 2024

References

1. Terryn, S., Brancart, J., Lefeber, D., Van Assche, G. & Vanderborght, B. Self-healing soft pneumatic robots. *Sci. Robot.* **2**, 16 (2017).
2. Kim, Y. I. I. et al. Nanotextured soft electrothermo-pneumatic actuator for constructing lightweight, integrated, and untethered soft robotics. *Soft Robot.* **9**, 960–969 (2022).
3. Hu, W. & Alici, G. Bioinspired three-dimensional-printed helical soft pneumatic actuators and their characterization. *Soft Robot.* **7**, 267–282 (2020).
4. De Pascali, C., Naselli, G. A., Palagi, S., Scharff, R. B. N. & Mazzolai, B. 3D-printed biomimetic artificial muscles using soft actuators that contract and elongate. *Sci. Robot.* **7**, 4155 (2022).
5. Correia, C. et al. Improving grasp function after spinal cord injury with a soft robotic glove. *IEEE Trans. Neural Syst. Rehabil. Eng.* **28**, 1407–1415 (2020).

6. Park, J., Choi, J., Kim, S. J., Seo, K. H. & Kim, J. Design of an inflatable wrinkle actuator with fast inflation/deflation responses for wearable suits. *IEEE Robot. Autom. Lett.* **5**, 3804–3810 (2020).
7. Yuk, H. et al. Hydraulic hydrogel actuators and robots optically and sonically camouflaged in water. *Nat. Commun.* **8**, 1–12 (2017).
8. Aubin, C. A. et al. Electrolytic vascular systems for energy-dense robots. *Nature* **571**, 51–57 (2019).
9. Ji, X. et al. An autonomous untethered fast soft robotic insect driven by low-voltage dielectric elastomer actuators. *Sci. Robot.* **4**, eaaz6451 (2019).
10. Gu, G., Zou, J., Zhao, R., Zhao, X. & Zhu, X. Soft wall-climbing robots. *Sci. Robot.* **3**, eaat2874 (2018).
11. Ju, Y. et al. Reconfigurable magnetic soft robots with multimodal locomotion. *Nano Energy* **87**, 106169 (2021).
12. Wu, Y., Dong, X., Kim, J. K., Wang, C. & Sitti, M. Wireless soft millirobots for climbing three-dimensional surfaces in confined spaces. *Sci. Adv.* **8**, 3431 (2022).
13. Sanchez, V. et al. Smart thermally actuating textiles. *Adv. Mater. Technol.* **5**, 2000383 (2020).
14. Li, S. et al. Digital light processing of liquid crystal elastomers for self-sensing artificial muscles. *Sci. Adv.* **7**, 3677–3700 (2021).
15. Kotal, M. et al. Highly bendable ionic soft actuator based on nitrogen-enriched 3D hetero-nanostructure electrode. *Adv. Funct. Mater.* **28**, 1802464 (2018).
16. Yan, Y. et al. Electroactive ionic soft actuators with monolithically integrated gold nanocomposite electrodes. *Adv. Mater.* **29**, 1606109 (2017).
17. Rafsanjani, A., Zhang, Y., Liu, B., Rubinstein, S. M. & Bertoldi, K. Kirigami skins make a simple soft actuator crawl. *Sci. Robot.* **3**, eaar7555 (2018).
18. Jones, T. J., Jambon-Puillet, E., Marthelot, J. & Brun, P. T. Bubble casting soft robotics. *Nature* **599**, 229–233 (2021).
19. Kim, T. H., Bao, C., Chen, Z. & Kim, W. S. 3D printed leech-inspired origami dry electrodes for electrophysiology sensing robots. *NPJ Flex. Electron.* **6**, 1–10 (2022).
20. Sonar, H. A., Gerratt, A. P., Lacour, S. P. & Paik, J. Closed-loop haptic feedback control using a self-sensing soft pneumatic actuator skin. *Soft Robot.* **7**, 22–29 (2020).
21. Kan, Z., Pang, C., Zhang, Y., Yang, Y. & Wang, M. Y. Soft actuator with programmable design: modeling, prototyping, and applications. *Soft Robot.* **9**, 907–925 (2022).
22. Nguyen, P. H. & Zhang, W. Design and computational modeling of fabric soft pneumatic actuators for wearable assistive devices. *Sci. Rep.* **10**, 1–13 (2020).
23. Proietti, T. et al. Sensing and control of a multi-joint soft wearable robot for upper-limb assistance and rehabilitation. *IEEE Robot. Autom. Lett.* **6**, 2381–2388 (2021).
24. Zhao, H., O'Brien, K., Li, S. & Shepherd, R. F. Optoelectronically innervated soft prosthetic hand via stretchable optical waveguides. *Sci. Robot.* **1**, eaai7529 (2016).
25. Yang, Y. & Chen, Y. Innovative design of embedded pressure and position sensors for soft actuators. *IEEE Robot. Autom. Lett.* **3**, 656–663 (2018).
26. Thuruthel, T. G., Shih, B., Laschi, C. & Tolley, M. T. Soft robot perception using embedded soft sensors and recurrent neural networks. *Sci. Robot.* **4**, 1488 (2019).
27. Lin, Y.-H. et al. Modeling and control of a soft robotic fish with integrated soft sensing. *Adv. Intell. Syst.* **5**, 2000244 (2021).
28. Bao, C., Kim, T. H., Hassanpoor Kalhori, A. & Kim, W. S. A 3D-printed neuromorphic humanoid hand for grasping unknown objects. *iScience* **25**, 104119 (2022).
29. Robinson, S. S. et al. Integrated soft sensors and elastomeric actuators for tactile machines with kinesthetic sense. *Extrem. Mech. Lett.* **5**, 47–53 (2015).
30. Kim, T.-H. et al. 3D origami sensing robots for cooperative healthcare monitoring. *Adv. Mater. Technol.* **6**, 2000938 (2021).
31. Kaur, M. & Kim, W. S. Toward a smart compliant robotic gripper equipped with 3D-designed cellular fingers. *Adv. Intell. Syst.* **1**, 1900019 (2019).
32. Kim, W., Park, H. & Kim, J. Compact flat fabric pneumatic artificial muscle (ffPAM) for soft wearable robotic devices. *IEEE Robot. Autom. Lett.* **6**, 2603–2610 (2021).
33. Mirzanejad, H. & Agheli, M. Soft force sensor made of magnetic powder blended with silicone rubber. *Sens. Actuators A Phys.* **293**, 108–118 (2019).
34. Xing, Z., Lin, J., McCoul, D., Zhang, D. & Zhao, J. Inductive strain sensor with high repeatability and ultra-low hysteresis based on mechanical spring. *IEEE Sens. J.* **20**, 14670–14675 (2020).
35. Kim, T. et al. Heterogeneous sensing in a multifunctional soft sensor for human-robot interfaces. *Sci. Robot.* **5**, 6878 (2020).
36. Larson, C. et al. Highly stretchable electroluminescent skin for optical signaling and tactile sensing. *Science* **351**, 1071–1074 (2016).
37. Bai, H., Kim, Y. S. & Shepherd, R. F. Autonomous self-healing optical sensors for damage intelligent soft-bodied systems. *Sci. Adv.* **8**, eabq2104 (2022).
38. Chen, W., Xiong, C., Liu, C., Li, P. & Chen, Y. Fabrication and dynamic modeling of bidirectional bending soft actuator integrated with optical waveguide curvature sensor. *Soft Robot.* **6**, 495–506 (2019).
39. Gerboni, G., Diodato, A., Ciuti, G., Cianchetti, M. & Menciassi, A. Feedback control of soft robot actuators via commercial flex bend sensors. *IEEE/ASME Trans. Mechatron.* **22**, 1881–1888 (2017).
40. Truby, R. L. et al. Soft somatosensitive actuators via embedded 3D printing. *Adv. Mater.* **30**, 1706383 (2018).
41. Mete, M. & Paik, J. Closed-loop position control of a self-sensing 3-DoF origami module with pneumatic actuators. *IEEE Robot. Autom. Lett.* **6**, 8213–8220 (2021).
42. Yang, T. H., Shintake, J., Kanno, R., Kao, C. R. & Mizuno, J. Low-cost sensor-rich fluidic elastomer actuators embedded with paper electronics. *Adv. Intell. Syst.* **2**, 2000025 (2020).
43. Daerden, F. & Lefeber, D. Pneumatic Artificial Muscles: actuators for robotics and automation. *Eur. J. Mech. Environ. Eng.* **47**, 11–21 (2002).
44. Polygerinos, P., Wang, Z., Galloway, K. C., Wood, R. J. & Walsh, C. J. Soft robotic glove for combined assistance and at-home rehabilitation. *Robot. Auton. Syst.* **73**, 135–143 (2015).
45. Polygerinos, P. et al. Modeling of soft fiber-reinforced bending actuators. *IEEE Trans. Robot.* **31**, 778–789 (2015).
46. Wang, Z. et al. Interaction forces of soft fiber reinforced bending actuators. *IEEE/ASME Trans. Mechatronics* **22**, 717–727 (2017).
47. Prashanth, S. et al. Sensorized foam actuator with intrinsic proprioception and tunable stiffness behavior for soft robots. *Adv. Intell. Syst.* **3**, 2100022 (2021).
48. Robertson, M. A. & Paik, J. New soft robots really suck: vacuum-powered systems empower diverse capabilities. *Sci. Robot.* **2**, 6357 (2017).
49. Tawk, C. & Alici, G. A review of 3D-printable soft pneumatic actuators and sensors: research challenges and opportunities. *Adv. Intell. Syst.* **3**, 2000223 (2021).
50. Umeno, T., Kaneko, T. & Hori, Y. Robust servosystem design with two degrees of freedom and its application to novel motion control of robot manipulators. *IEEE Trans. Ind. Electron.* **40**, 473–485 (1993).
51. Samuel, K., Haninger, K., Oboe, R. & Oh, S. Integrated disturbance observer-based robust force control. *IEEE Trans. Ind. Electron.* **70**, 11483–11494 (2023).

Acknowledgements

This work was supported by the National Research Foundation of Korea (NRF) grant funded by the Korea government (MSIT) (No. NRF-2021R1C1C1009271

and NRF-2022R1A4A3033320). This research was also supported by the Development of technologies for electroceuticals of the National Research Foundation (NRF) funded by the Korean government (MSIT) (No. NRF-2022M3E5E9017837). Finally, This work was supported by the Industrial Fundamental Technology Development Program (20018274, Development of gripper system for various production processes and multi-modal flexible tactile sensor system) funded by the Ministry of Trade, Industry & Energy (MOTIE) of Korea.

Author contributions

H.K. conducted the overall experiments, measurements, and analysis and wrote the manuscript. H.N. and T.K. designed the algorithm for the demonstration of a closed-loop control system. S.N. performed the computational simulation for the mechanical behavior of the soft actuator and microfiber-based flexible proprioceptive bending sensor. S.C., G.S., and C.L. fabricated the circuits for the operation of the gripping system. J.K. and S.L. provided assistance on the fabrication of the proprioceptive sensing system. Y.P., S.O., and J.L. supervised the project.

Competing interests

The authors declare no competing interests.

Additional information

Supplementary information The online version contains supplementary material available at https://doi.org/10.1038/s41528-024-00302-6.

Correspondence and requests for materials should be addressed to Jaehong Lee.